Fresnel diffraction effects in Fourier-transform arrayed waveguide grating spectrometer

J. A. Rodrigo[1], P. Cheben[2], T. Alieva[1], M. L. Calvo[1], M. Florjańczyk[3], S. Janz[2], A. Scott[4], B. Solheim[3], D.-X. Xu[2], and A. Delâge[2]

[1]*Departamento de Óptica, Fac. de C. Físicas, Universidad Complutense de Madrid, 28040 Spain;*

[2]*Institute for Microstructural Sciences, National Research Council, Ottawa, K1A 0R6 Canada;*

[3]*CRESS Space Instrumentation Laboratory, York University, Toronto M3J1P3 Canada;*

[4] *COMDEV Ltd., Ottawa, K2K3J1 Canada*
jarmar@fis.ucm.es

Abstract: We present an analysis of Fourier-transform arrayed waveguide gratings in the Fresnel diffraction regime. We report a distinct spatial modulation of the interference pattern referred to as the Moiré-Talbot effect. The effect and its influence in a FT AWG device is explained by deriving an original analytical expression for the modulated field, and is also confirmed by numerical simulations using the angular spectrum method to solve the Fresnel diffraction integral. We illustrate the retrieval of spectral information in a waveguide Fourier-transform spectrometer in the presence of the Moiré-Talbot effect. The simulated device comprises two interleaved waveguide arrays each with 180 waveguides and the interference order of 40. It is designed with a Rayleigh spectral resolution of 0.1 nm and 8 nm bandwidth at wavelength $\lambda \sim 1.5$ μm. We also demonstrate by numerical simulations that the spectrometer crosstalk is reduced from -20 dB to -40 dB by Gaussian apodization.

OCIS codes: (130.1750) integrated optics: components; (130.3120) integrated optics: integrated optics devices; (230.7390) optical devices: waveguides, planar; (230.7380) optical devices: waveguides, channeled; (250.5300) optoelectronics: photonic integrated circuits; (050.0050) diffraction and gratings.

References and links

1. P. Cheben, "Wavelength dispersive planar waveguide devices: Echelle gratings and arrayed waveguide gratings," in Optical Waveguides: From Theory to Applied Technologies, Eds. M. L. Calvo and V. Laksminarayanan, Chapter 5, CRC Press, London, (2007).
2. P. Cheben, J. H. Schmid, A. Delâge, A. Densmore, S. Janz, B. Lamontagne, J. Lapointe, E. Post, P. Waldron, and D.-X. Xu, "A high-resolution silicon-on-insulator arrayed waveguide grating microspectrometer with submicrometer aperture waveguides," Opt. Express **15**, 2299-2306 (2007).
3. P. Jacquinot, "The luminosity of spectrometers with prisms, gratings, or Fabry Perot etalons," J. Opt. Soc. Am. **44**, 761 (1954).
4. P.B. Fellgett, PhD Thesis, University of Cambridge, (1951).

#87916 - $15.00 USD Received 25 Sep 2007; revised 20 Nov 2007; accepted 20 Nov 2007; published 27 Nov 2007

5. P. Cheben, I. Powell, S. Janz, and D.-X. Xu, "Wavelength-dispersive device based on a Fourier-transform Michelson-type arrayed waveguide grating," Opt. Lett. **30**, 1824-1826 (2005).
6. J. M. Harlander, F. L. Roesler, Ch. R. Englert, J. G. Cardon, R. R. Conway, Ch. M. Brown, and J. Wimperis, "Robust monolithic ultraviolet interferometer for the SHIMMER instrument on STPSat-1," Appl. Opt. **42**, 2829-2834 (2003).
7. M. Florjańczyk, P. Cheben, S. Janz, A. Scott, B. Solheim, and D.-X. Xu, Planar waveguide spatial heterodyne spectrometer, Proc. Photonics North Conference, 4-7 June, 2007, Ottawa, Canada.
8. P. Cheben, A. Delâge, L. Erickson, S. Janz, and D.-X. Xu, "Polarization compensation in silicon-on-insulator arrayed waveguide grating devices," in Silicon-based and hybrid optoelectronics III, SPIE Proc. 4293, 15-22, (2001).
9. P. Cheben, D.-X. Xu, S. Janz, A. Delâge, and D. Dalacu, "Birefringence compensation in silicon-on-insulator planar waveguide demultiplexers using a buried oxide layer," in Optoelectronic Integration on Silicon, SPIE Proc. 4997, 181-189, (2003).
10. M. K. Smit and C. van Dam, "Phasar-based WDM-devices: principles, design, and applications," IEEE J. Sel. Top. Quantum Electron., **2**, 236 (1996).
11. D. Mendlovic, Z. Zalevsky, and N. Konforti, "Computation considerations and fast algorithms for calculating the diffraction integral," J. Mod. Opt. **44**, 407 (1997).
12. H. Hamam and J. L. De Bougrenet de la Tocnaye, "Programmable joint fractional Talbot computer-generated holograms," J. Opt. Soc. Am. A **12**, 314 (1995).
13. H. Hamam and J. L. de Bougrenet de la Tocnaye, "Efficient Fresnel transform algorithm based on fractional Fresnel diffraction," J. Opt. Soc. Am. A **12**, 1920 (1995).

1. Introduction

Waveguide spectrometers such as waveguide echelle gratings and arrayed waveguide gratings (AWGs) [1] are key devices in optical telecommunication networks, where they perform functions such as wavelength multiplexing (WDM), wavelength filtering, and signal routing. New applications are emerging in optical interconnects, spectroscopy, metrology, and chemical and biological sensing. In order to meet high spectral resolution demanded by some applications, a compact spectrometer chip has been demonstrated with many channels and a high spectral resolution by using high index contrast (HIC) silicon-on-insulator (SOI) waveguides [2].

Spectroscopic monitoring and sensing applications that detect low-power optical signals may present additional challenges to high resolution. In such devices, often a figure of merit to be maximized is the optical throughput, or *étendue*. Jacquinot was first to notice that large *étendue* is an intrinsic property of a Michelson interferometer [3]. Together with Fellgett multiplex advantage [4], the Jacquinot advantage is the main reason why Fourier-transform Michelson interferometers are currently dominating the field of infrared spectroscopy.

In order to exploit the *étendue* benefit of a Michelson interferometer, we proposed the first Fourier-transform Michelson-type arrayed waveguide grating (AWG) spectrometer [5]. This device further develops the concept by Harlander et al. who proposed replacing the mirrors in a Michelson interferometer by bulk optics diffraction gratings [6]. Compared to a conventional AWG which is a generalized multi-path Mach-Zehnder interferometer, our FT AWG, as a Michelson-type device, allows for a markedly larger input aperture with a correspondingly increased optical throughput. Furthermore, unlike a conventional Fourier-transform Michelson spectrometer which requires moving parts (a scanning mirror), the FT AWG is a static device obviating the need for scanning elements.

The FT waveguide spectrometer concept can be further generalized to include various waveguide configurations in transmissive and reflective geometries. Recently, a multi-aperture configuration has been proposed [7]. By simultaneously using multiple input apertures, the optical throughput is largely increased.

In this work we discuss the near field diffraction effects in a Fourier-transform AWG microspectrometer in a transmission geometry. In contrast to conventional AWG devices where an image of the input waveguide is formed dispersively in the focal region, thus operating in Frauhoffer (far field) diffraction regime, our device does not involve focusing and operates in

#87916 - $15.00 USD Received 25 Sep 2007; revised 20 Nov 2007; accepted 20 Nov 2007; published 27 Nov 2007

Fresnel regime. This requires to solve the near-field diffraction problem, and this is the first time it is addressed for an AWG device. We show that each waveguide array of the interleaved AWG produces in the combiner free propagation region its distinct spatial Talbot effect and the superposition of these Talbot patterns yields a spatial Moiré pattern. We explain the effect analytically and also study it numerically, including its influence in a FT AWG spectrometer device.

2. Moiré-Talbot effect in Fourier-transform AWG devices

The schematic of an FT AWG device is shown in Fig. 1. The input field is sampled by a multiple waveguide aperture followed by an array of 3 dB splitters which couple light into two interleaved waveguide arrays AWG$_p$ ($p = 1,2$) with respective interference orders m_p. The required linear optical path increment between the adjacent waveguides of each AWG are obtained with bend waveguide sections acting as phase shifters, as indicated in Fig. 1. The bend waveguide sections are commonly used in planar waveguide devices. All parts of the device, including bend waveguide sections, are contained within the waveguide plane (Fig. 1, plane *xz*). The waveguide pairs of the two AWGs can be recombined by an array of 3 dB couplers, forming a multiple waveguide output aperture terminated in the slab waveguide combiner region followed by the free-propagating region (air). In the schematic shown in Fig. 1, the fringes are intercepted directly by a phototedector array located at the chip edge. Optionally, the fringes can be sampled by an array of receiver channel waveguides (Fig. 1), as it is discussed at the end of Section 2. Full details of such generalized Mach-Zehnder approach have been published elsewhere [7].

Though this is a theoretical work and no device has yet been fabricated, the FT AWG can be implemented on different planar waveguides, including low− and high−index−contrast platforms. In this paper we show a design example for a silicon-on-insulator (SOI) waveguide platform which we previously used for fabricating compact AWG devices [8, 9].

For interleaved AWGs with inverted interference orders ($m_1 = -m_2 = m$), as the wavelength changes, the two wavefronts emerging at the output aperture of the respective waveguide arrays tilt in the opposite direction according to the AWG dispersion relation. This superposition results in interference fringes with a wavelength-dependent period in the combiner free propagation region where the two wavefronts overlap. In the combiner region, wavefront W_p originating from AWG$_p$ propagates with a wavelength dependent tilt angle $\beta(\lambda)$. The latter is a function of the phase shift $\Delta\phi(\lambda)$ between the wavelets originating in the two adjacent waveguides of an AWG that can be expressed as [1, 10]:

$$|\Delta\phi| = \left| \frac{2\pi m_p n_g (\lambda - \lambda_L)}{n_0 \lambda_L} \right| \tag{1}$$

and the wavefront tilt angle β:

$$\sin\beta = (\lambda - \lambda_L) \frac{n_g m_p}{d\, n_0 n_{eff}}, \tag{2}$$

where λ_L is the Littrow wavelength, n_g is the group index of the arrayed waveguides, n_0 is the fundamental waveguide mode effective index, n_{eff} is the effective index in the combiner region, and d is the AWG pitch [5].

The scalar field distribution in proximity of the waveguide array can be obtained by solving the diffraction problem in the Fresnel regime for the periodic waveguide grating structure. The field at the interface between the waveguide array and the combiner region can be represented by the periodic signal $t(x)$ with a tilted phase front:

#87916 - $15.00 USD Received 25 Sep 2007; revised 20 Nov 2007; accepted 20 Nov 2007; published 27 Nov 2007

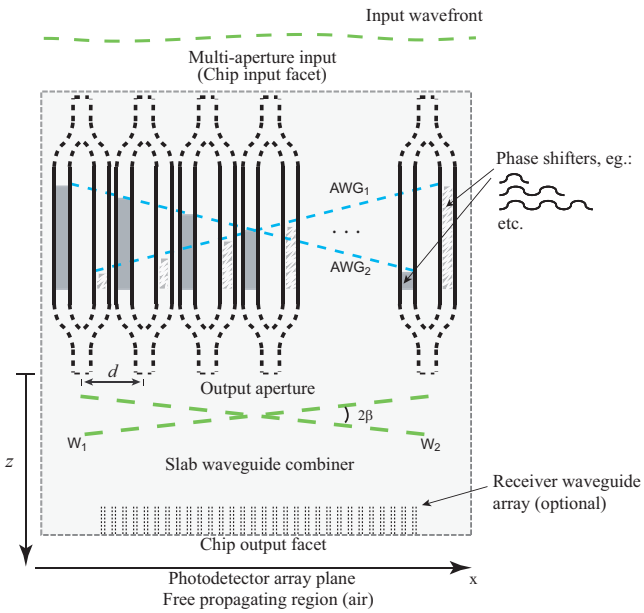

Fig. 1. General schematics of a FT AWG microspectrometer with two interleaved AWGs. Wavefronts W_1 and W_2 originating from AWG_1 and AWG_2 propagate with a wavelength dependent tilt angle $\beta(\lambda)$ and $-\beta(\lambda)$, respectively.

$$T_p(x) = t(x)\exp(-i2\pi\alpha_p x), \tag{3}$$

where

$$t(x) = \sum_{q=-\infty}^{+\infty} a_q \exp\left(i2\pi\frac{qx}{d}\right) \tag{4}$$

is one dimensional Fourier expansion and $\alpha_p = \sin(\beta)/\lambda$. For an FT device with interleaved AWGs, $\alpha_1 = -\alpha_2 = \alpha$ and $T_1(x) = T_2^*(x) = T(x)$. The field distribution at a distance z from the waveguide array aperture is given by the Fresnel integral:

$$\begin{aligned} W_p(x,\,z) &= \frac{\exp(ikn_{eff}z)}{\sqrt{i\lambda z}}\int_{-\infty}^{\infty} T_p(x_i)\exp\left(i\frac{\pi n_{eff}}{\lambda z}(x-x_i)^2\right)dx_i \\ &= \Phi(z)\exp(-i2\pi\alpha_p x)\sum_{q=-\infty}^{+\infty} a_q \exp\left(i2\pi\frac{qx}{d}\right)\exp\left(-i\pi\lambda z\frac{q^2}{d^2 n_{eff}}\right)\exp\left(i2\pi\lambda z\alpha_p\frac{q}{dn_{eff}}\right), \end{aligned} \tag{5}$$

where

$$\Phi(z) = \exp(ikn_{eff}z)\exp\left(-i\pi\lambda z\alpha_p^2/n_{eff}\right). \tag{6}$$

At the propagation distance $z_l = z_T l$ ($l = 1, 2\ldots$), Eq. (5) is reduced to:

$$\begin{aligned} W_p(x,z_l) &= \Phi(z_l)t\left(x+2d^2 l\alpha_p\right)\exp(-i2\pi\alpha_p x) \\ &= \Phi(z_l)T_p\left(x+2d^2 l\alpha_p\right)\exp(i2\pi 2\left(d\alpha_p\right)^2 l). \end{aligned} \tag{7}$$

#87916 - $15.00 USD Received 25 Sep 2007; revised 20 Nov 2007; accepted 20 Nov 2007; published 27 Nov 2007

Eq. (7) represents the well-known Talbot effect, also known as self-imaging phenomenon, with the Talbot distance $z_T = 2n_{eff}d^2/\lambda$.

The interference pattern at the propagation distance $z_T l$ is given by:

$$I(x,z_T l) = |W_1(x,z_T l) + W_2(x,z_T l)|^2 = \left|t\left(x+2d^2 l\alpha\right) + t\left(x-2d^2 l\alpha\right)\exp(i2\pi 2\alpha x)\right|^2$$
$$= \left|t\left(x+2d^2 l\alpha\right)\right|^2 + \left|t\left(x-2d^2 l\alpha\right)\right|^2 + 2t\left(x+2d^2 l\alpha\right)t\left(x-2d^2 l\alpha\right)\cos(2\pi 2\alpha x). \quad (8)$$

It is straightforward to show that Eq. (8) contains various terms with wavelength dependent spatial frequencies of 2α, $f_d \pm 2\alpha j$ and $2f_d \pm 2\alpha j$, where $j = 0$ or 1, and $f_d = 1/d$ is the spatial frequency of the single waveguide array.

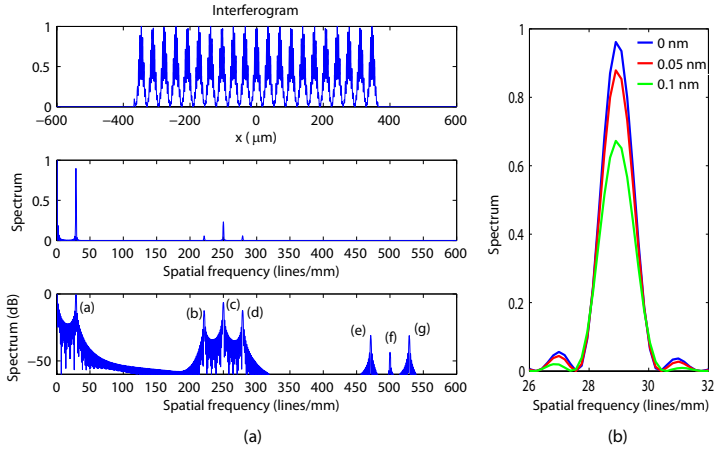

Fig. 2. Interferogram (top) at a Talbot plane and its Fourier spectrum (center and bottom, in linear and logarithmic scales, respectively). Wavelength $\lambda = 1502$ nm. The peaks (a-g) correspond to the spatial frequencies of 2α (a), $f_d \pm 2\alpha j$ (b-d) and $2f_d \pm 2\alpha j$ (e-g). Right panel shows the calculated spectra for the input light with spectral widths (FWHM) of $\Delta\lambda = 0$ nm (monochromatic), 0.05 nm and 0.1 nm.

The nature of the terms with different spatial frequencies in Eq. (8) is illustrated in the following example. Let us consider an interleaved FT AWG device, with 180 waveguides in each of the array, hence total $N = 360$ waveguides, and interference order $m_1 = -m_2 = 40$. The pitch at the arrayed waveguide aperture is $d = 4$ μm, and the effective width of the waveguide fundamental mode is $w = 4.8$ μm. The total number of waveguides (N) and the interference order (m) were chosen to provide the specified spectral resolution ($\Delta\lambda = 0.1$ nm at Rayleigh limit). We showed previously [5] that in a Fourier transform arrayed waveguide spectrometer the wavelength resolution is $\Delta\lambda = \lambda/(mN)$, which is equivalent to a diffraction grating based device with N grating facets and the interference order m. The waveguide pitch d and the effective width of the waveguide mode was chosen based on our previous experimental work on AWGs fabricated in silicon-on-insulator (SOI) waveguide platform with a 2.2 μm-thick Si waveguide core layer [8, 9]. However, the pitch can be modified to provide a specific value of the FT AWG dispersion, according to Eq. (8). It's influence on the interference pattern is analytically included in Eq. (8) through the terms d and α, which also is a function of d. Figure 3 shows the influence of d on spectral retrieval for three device, with a pitch of 3 μm, 4 μm, and 5 μm, respectively. It is observed that as the pitch decreases, device dispersion increases, as in a conventional AWG. The terms (a)-(g) of Eq. (8) are also identified in Fig. 3 to help visualize the effect of varying pitch on different spatial frequencies in the Fourier spectrum.

#87916 - $15.00 USD Received 25 Sep 2007; revised 20 Nov 2007; accepted 20 Nov 2007; published 27 Nov 2007

Since $\alpha(\lambda_L) = 0$, there is obviously no spatial interference effect at the Littrow wavelength, which has been set here to $\lambda_L = 1500$ nm. Fig. 2 shows the interference pattern represented by Eq. (8) and its Fourier spectrum calculated by means of the FFT algorithm (Fast Fourier Transform) for the wavelength of 1502 nm. The spatial spectrum reveals seven peaks which correspond to the spatial frequencies of 2α (a), $f_d \pm 2\alpha j$ (b, c, d), and $2f_d \pm 2\alpha j$ (e, f, g), as they are identified in the bottom panel of Fig. 2. The terms corresponding to the peaks (a), (b), (d), (e), and (g) carry the spectral information, whereas the terms (c) and (f) represents the Talbot effect. It is important to clearly distinguish between these different terms since, if not correctly understood, they can be misinterpreted as spurious spectral lines. In this particular example the higher order terms (b)−(g) appear at rather high spatial frequencies thus would be automatically filtered when reading out the fringe pattern by a conventional photodetector array. However, in designs with the higher order terms at lower spatial frequencies, these would need to be carefully considered to avoid a false spectral interpretation. The influence of finite input light spectral width on the spectral resolution is shown in Fig. 2, right panel. It is observed that with an increasing width of the input light Gaussian distribution (0 nm, 0.05 nm, and 0.1 nm, FWHM), the calculated spectra are well resolved. Some decrease in the peak intensity and an increase in linewidth broadening with an increasing input light spectral width are observed.

The interference effect in the combiner and the free propagation regions is shown in Fig. 4, representing a scalar optical field calculated from the Fresnel integral using the angular spectrum method [11]. This method offers a fast and an accurate approximation to the Fresnel integral for generalized diffraction geometries. The wavefront propagation simulation starts at the arrayed waveguide output aperture ($z = 0$) and terminates at $z = 250$ μm. The combiner region is a silicon slab waveguide with $n_{eff} = 3.44$ for $0 < z < 125$ μm. The combiner is followed by a free propagation region (air) with $n_{eff} = 1$ for 125 μm $< z < 250$ μm.

Fig. 4 (a) shows the interference fringes at the Littrow wavelength of $\lambda_L = 1500$ nm, yielding the conventional Talbot effect. The inset shows the well known frequency doubling effect at the fractional Talbot plane $z = z_T/4$. Fig. 4 (b) shows the Moiré superposition of two Talbot effects for a wavelength of $\lambda = 1508$ nm.

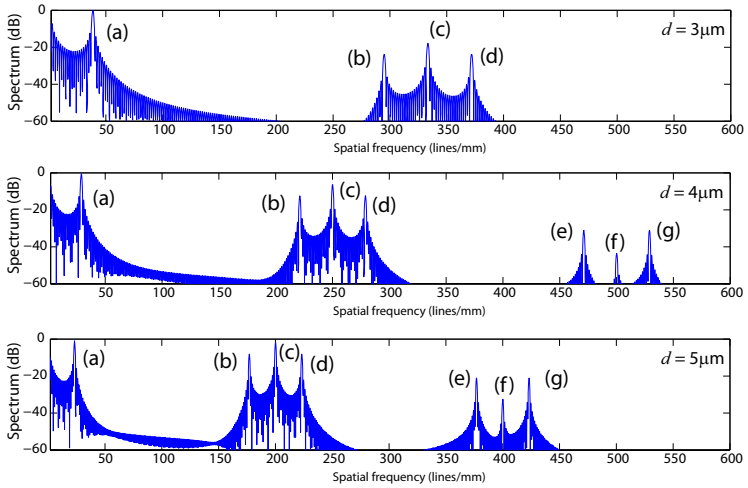

Fig. 3. The waveguide pitch influence on spectral retrieval. The waveguide pitch 3 μm (top), 4 μm (center), and 5 μm (bottom). The terms (a)-(g) of Eq. (8) are identified to help visualize the effect of varying pitch on different spatial frequencies.

Finally, we calculate interferogram and spectrum for a FT AWG device with the parameters

#87916 - $15.00 USD Received 25 Sep 2007; revised 20 Nov 2007; accepted 20 Nov 2007; published 27 Nov 2007

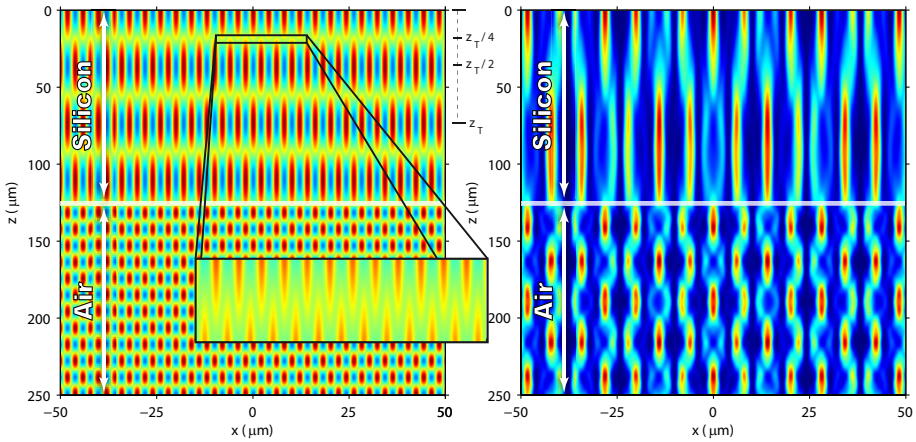

Fig. 4. Light interference in the combiner (silicon) and the free propagation (air) regions. a) Talbot effect at Littrow wavelength $\lambda_L = 1500$ nm; b) Moiré-Talbot effect at $\lambda = 1508$ nm. The silicon-air interface (spectrometer chip edge) is located at $z = 125$ μm, as it is indicated by the grey line in (a) and (b). Inset in figure (a) shows the intensity distribution at the fractional Talbot plane $z_T/4$.

described above, for the input light comprising several monochromatic spectral lines, namely of wavelengths, 1502 nm, 1502.3 nm, 1504 nm, 1505 nm, 1506 nm and 1508 nm. We assume that the interference pattern is sampled with a maximum spatial resolution of 130 lines/mm. Figure 5 and 6 show the interference pattern (top panel) calculated from Eq. (8) and its Fourier spectrum (central and bottom panels) for unapodized and Gaussian apodized input fields, respectively. The Gaussian apodization window has a width of $w_0 = 250$ μm.

It is observed that the two spectral lines separated by $\Delta\lambda = 0.3$ nm are resolved well beyond the Rayleigh criterion. The Rayleigh resolution is $\Delta\lambda = \lambda/R = \lambda/mN$ where m is interference order and N is the total number of interleaved waveguides, that in our device yields $\Delta\lambda \sim 0.1$ nm. The calculated spectra show that the microspectrometer crosstalk is reduced from -20 dB to -40 dB by Gaussian aperture apodization.

Similar results are obtained when the interferogram is registered at the fractional Talbot distances $z_T\eta/\zeta$, where η and ζ are integers and $\eta < \zeta$. The field distribution at the fractional distances $z_T\eta/\zeta$ is given by (ζ even):

$$W_p(x, z_T\eta/\zeta) = \Phi(z_T\eta/\zeta)\sum_{a=0}^{\zeta/2-1} B(a,\eta,\zeta)T_p\left(x - \frac{d}{2} + \frac{2\eta a}{\zeta}d + \frac{2\eta}{\zeta}d^2\alpha_p\right), \qquad (9)$$

where

$$B(a,\eta,\zeta) = \frac{2}{\zeta}\sum_{b=0}^{\zeta/2-1}\exp\left(i2\pi\frac{2ba}{\zeta}\right)\exp\left(-i\pi\left(2\frac{b^2\eta}{\zeta} + b\right)\right) \qquad (10)$$

are the Talbot coefficients. Equation Eq. (9) is a generalization of the expression obtained in [12] for small oblique angle of illumination (β). Analogously a relation for odd fractional orders ζ can be found, [13]. Therefore the field distribution at the fractional Talbot distance $z_T/2$ corresponds to

$$W_p(x, z_T/2) = \Phi(z_T/2)T_p\left(x - d/2 + d^2\alpha_p\right), \qquad (11)$$

whereas for the distance $z_T/4$ the field W_p is written as follows:

#87916 - $15.00 USD Received 25 Sep 2007; revised 20 Nov 2007; accepted 20 Nov 2007; published 27 Nov 2007

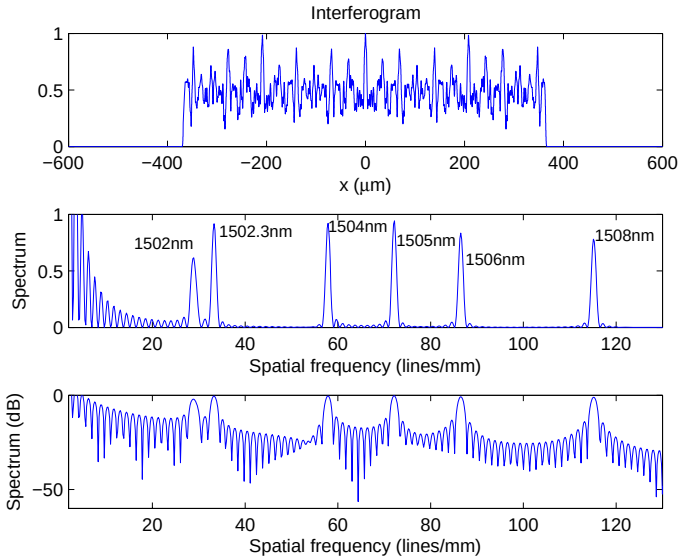

Fig. 5. Interferogram and calculated spectrum for an FT AWG device. Unapodized input field. The interferogram is at the Talbot plane $z = z_T$ (top), calculated from Eq. (8). Calculated spectrum (using the FFT algorithm) for wavelengths: 1502 nm, 1502.3 nm, 1504 nm, 1505 nm, 1506 nm and 1508 nm in linear (center) and logarithmic (bottom) scales.

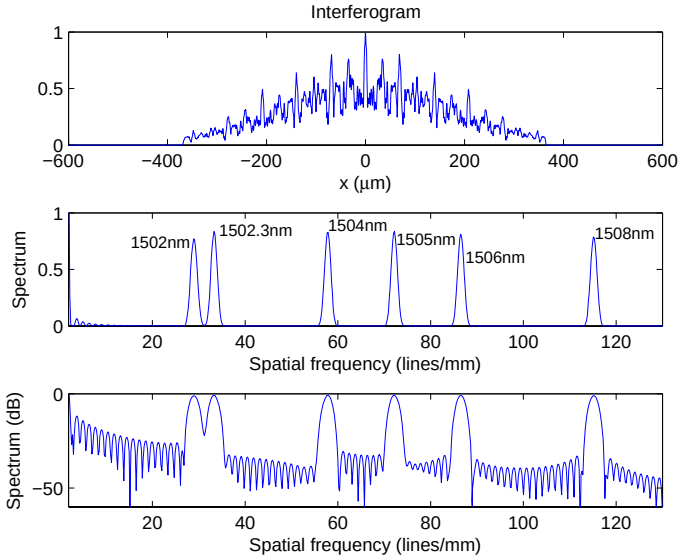

Fig. 6. Interferogram and calculated spectrum for FT AWG device. Gaussian apodized input field. The interferogram is at Talbot plane $z = z_T$ (top), calculated from Eq. (8). Calculated spectrum (using the FFT algorithm) for wavelengths: 1502 nm, 1502.3 nm, 1504 nm, 1505 nm, 1506 nm and 1508 nm in linear (center) and logarithmic (bottom) scales.

#87916 - $15.00 USD Received 25 Sep 2007; revised 20 Nov 2007; accepted 20 Nov 2007; published 27 Nov 2007

$$W_p(x,z_T/4)=\Phi(z_T/4)\sum_{a=0}^{1}B(a,1,4)T_p\left(x-\frac{d}{2}+\frac{a}{2}d+\frac{1}{2}d^2\alpha_p\right)$$
$$=\frac{\Phi(z_T/4)}{\sqrt{2}}\left(\exp(i\pi/4)\,T_p\left(x-\frac{d}{2}+\frac{d^2\alpha_p}{2}\right)+\exp(-i\pi/4)\,T_p\left(x+\frac{d^2\alpha_p}{2}\right)\right). \qquad (12)$$

Eq. (11) corresponds to the self-image of the array grating shifted by half period ($d/2$), thus the same conclusions previously explained for Eq. (7) are obtained. On the other hand, Eq. (12) corresponds to a frequency doubling effect which is shown in the inset of Fig. 4 (a) for the Littrow wavelength ($\alpha(\lambda_L)=0$).

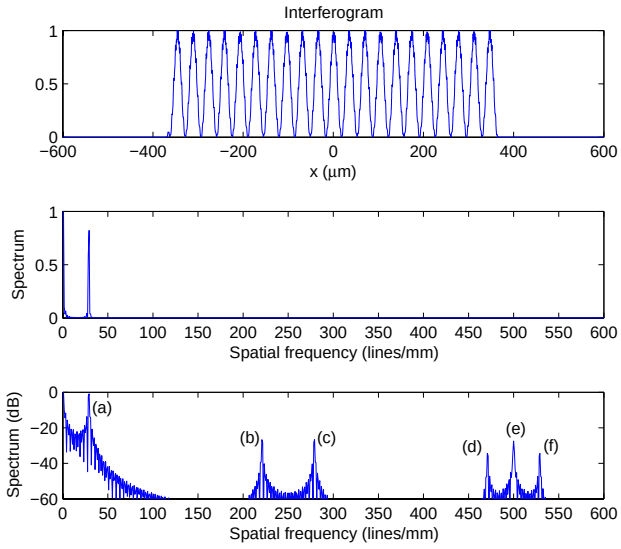

Fig. 7. Interferogram (top) at the fractional Talbot plane $z_T/4$ calculated from Eq. (14) and its Fourier spectrum (center and bottom, in linear and logarithmic scales, respectively). Unapodized input field. Wavelength $\lambda=1502$ nm. The peaks (a-f) correspond to the spatial frequencies of 2α (a), $f_d\pm 2\alpha$ (b,c) and $2f_d\pm 2\alpha j$ (d-f).

The interferogram at this fractional Talbot distance is given by the expression:

$$I(x,z_T/4) = \frac{1}{2}\left|\exp(i\pi/4)\left[T_1\left(x-\frac{d}{2}+\frac{d^2\alpha}{2}\right)+T_2\left(x-\frac{d}{2}-\frac{d^2\alpha}{2}\right)\right]\right.$$
$$\left.+\exp(-i\pi/4)\left[T_1\left(x+\frac{d^2\alpha}{2}\right)+T_2\left(x-\frac{d^2\alpha}{2}\right)\right]\right|^2. \qquad (13)$$

In our case the condition $\alpha<1/d$ is satisfied and therefore Eq. (13) is simplified to

$$I(x,z_T/4)=(1+\cos(2\pi 2\alpha x))\times$$
$$\left|\exp(i\pi/4)\,t\left(x-\frac{d}{2}\right)\left[\cos(d\pi\alpha)+\tan(2\pi\alpha x)\sin(d\pi\alpha)\right]+\exp(-i\pi/4)\,t(x)\right|^2. \qquad (14)$$

#87916 - $15.00 USD Received 25 Sep 2007; revised 20 Nov 2007; accepted 20 Nov 2007; published 27 Nov 2007

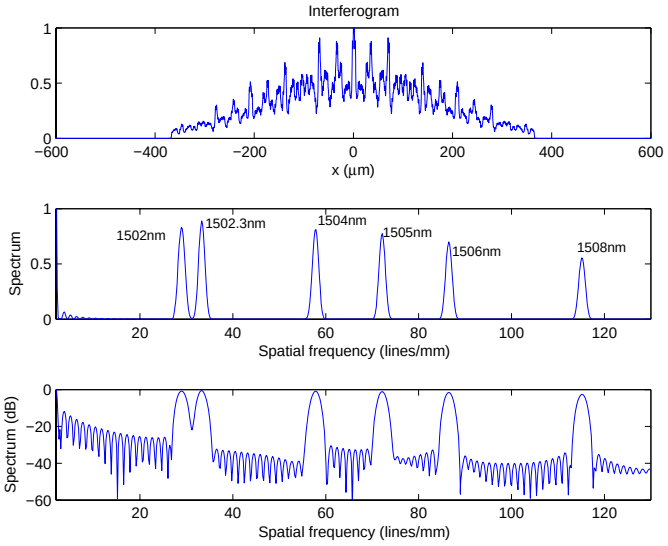

Fig. 8. Interferogram and calculated spectrum for FT AWG device. Gaussian apodized input field. The interferogram is at Talbot plane $z = z_T/4$ (top), calculated from Eq. (14). Calculated spectrum (using the FFT algorithm) for wavelengths: 1502 nm, 1502.3 nm, 1504 nm, 1505 nm, 1506 nm and 1508 nm in linear (center) and logarithmic (bottom) scales.

This interferogram also contains various terms with wavelength dependent spatial frequencies of 2α, $f_d \pm 2\alpha$ and $2f_d \pm 2\alpha j$, $j = 0$ or 1, Fig. 7. In contrast to Eq. (8) (see Fig. 2), the interferogram represented by Eq. (14) does not contain the spatial frequency f_d due to the term: $\cos(d\pi\alpha) + \tan(2\pi\alpha x)\sin(d\pi\alpha)$, see Fig. 7 (1502 nm). Figure 8 shows the interference pattern (top panel) calculated from Eq. (14) and its Fourier spectrum (central and bottom panels) for Gaussian apodized input field, comprising several wavelengths: 1502 nm, 1502.3 nm, 1504 nm, 1505 nm, 1506 nm and 1508 nm. The crosstalk as well as the spectral line resolution $\Delta\lambda$ demonstrated in Fig. 8, are similar to the result obtained previously for the non fractional Talbot distance, displayed in Fig. 6.

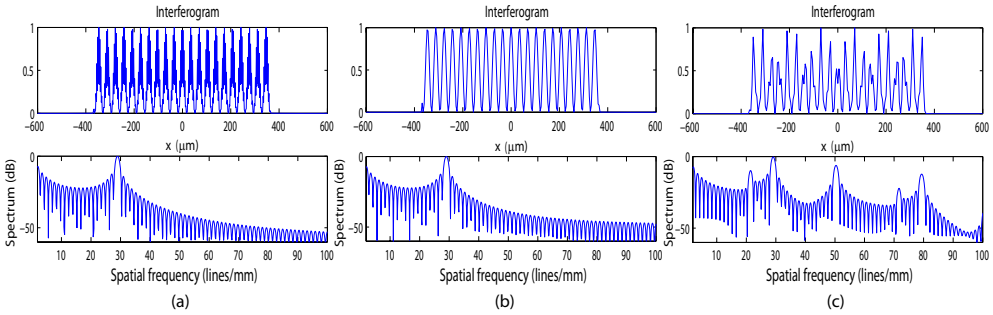

Fig. 9. Influence of interferogram sampling on spectrum retrieval. Gaussian unapodized input field. The interferogram (top) at Talbot plane $z = z_T$. Calculated spectra for the wavelength of 1502 nm and different sampling frequencies (bottom); sampling periods 2 μm (a), 4 μm (b) and 5 μm (c).

#87916 - $15.00 USD Received 25 Sep 2007; revised 20 Nov 2007; accepted 20 Nov 2007; published 27 Nov 2007

It should be noted that the distance z_T is a function of wavelength. If the interferogram is evaluated for example at Talbot plane $z = z_{T,L}$ at λ_L, at other wavelengths this position deviates by $\Delta z = z_{T,L}\ (\lambda - \lambda_L)/\ \lambda$. For the interleaved FT AWG device considered in this work, the maximum spatial shift is $\Delta z_{\max} = 0.4\ \mu$m which corresponds to the wavelength $\lambda = 1508$ nm and $n_{eff} = 3.44$ (silicon region). Because the Talbot distance $z_T(\lambda_L)$ is proportional to the effective index, this factor is reduced to $\Delta z_{\max} = 0.12\ \mu$m when the interferogram is registered in the air region, that is a comparatively small value. According to our calculations, the influence of this Talbot plane shift with wavelength on spectral retrieval is negligible. This is also evident comparing the spectra in Fig. 6 and Fig. 8. The two spectra are virtually identical, but they are retrieved at rather different positions, namely at z_T (Fig. 6) and $z_T/4$ (Fig. 8).

Though it is not required for understanding of the Fresnel diffraction effects in a FT AWG, here we will briefly consider the effect of interferogram sampling. Using an array of receiver waveguides is a convenient way to sample the interferogram. This is because the receiver waveguides can be designed with a pitch as small as $\sim 1\ \mu$m, which cannot be achieved with the state of the art photodetector array technologies. A further advantage of using the receiver waveguide array is that the waveguides can easily be fanned-out to a separation matching the pitch of the photodetector array. Figure 9 shows the influence of the interferometer sampling frequency on the spectral retrieval for an interference pattern sampled by an array of receiver waveguides with periods 2 μm, 4 μm, and 5 μm, respectively. No deterioration of the calculated spectrum is noticed up to the sampling period of 4 μm. For the sampling period of 5 μm, four satellite peaks appear in the calculated spectrum as the result of undersampling. Thus, for this device example, a spatial sampling period $\leq$4 μm suffices for accurate spectral retrieval. Such waveguide spacings can be routinely achieved using high-index contrast silicon-on-insulator waveguides. We have reported on design and fabrication of waveguide arrays with a pitch as small as 1 μm and a negligible loss and crosstalk [2]. An advantage of sampling the interference pattern by a waveguides array is that the waveguides can be conveniently fanned-out for a specific pitch of a conventional photodetector array facing the chip edge. Indeed, other techniques can also be used for sampling the interferogram. For example, the FT AWG dispersion can be designed such that the interferogram maximum spatial frequency is still resolved by the photodetector array. The FT AWG dispersion can be controlled by modifying the interference order *m* or waveguide pitch *d*, see Eq. (2). Alternatively, imaging optics at the chip output can be used to match the interference pattern to the pitch of the photodetector array.

3. Conclusions

We have discussed interference effects in a Fourier-transform arrayed waveguide grating device, namely a spatial modulation of the interference pattern that we refer to as the Moiré-Talbot effect. The origin of the effect was explained by an analytical formalism and was confirmed by numerical simulations. The effect has been demonstrated on a Fourier-transform device with interleaved waveguide arrays. Using the developed analytical formalism and numerical tools, a FT AWG device with Rayleigh resolution of $\Delta\lambda = 0.1$ nm, 8 nm bandwidth, and a Littrow wavelength of $\lambda = 1500$ nm was simulated. The crosstalk level reduction to -40 dB was demonstrated for a Gaussian apodized input field.

Acknowledgements

The financial support of the Spanish Ministry of Education and Science under project TEC2005-02180 and "Slab Waveguide Spatial Heterodyne Spetrometer project", Contract 9F028-064201/007/MTB, Space Technology Development Program, Canada Space Agency are acknowledged.

#87916 - $15.00 USD Received 25 Sep 2007; revised 20 Nov 2007; accepted 20 Nov 2007; published 27 Nov 2007